ISSN 2278-3091
Volume 10, No.3, May - June 2021
International Journal of Advanced Trends in Computer Science and Engineering
Available Online at http://www.warse.org/IJATCSE/static/pdf/file/ijatcse331032021.pdf
https://doi.org/10.30534/ijatcse/2021/331032021

Skin Lesions Detection and Classification Using Deep Learning

Waqas Rizwan[1], Syed Muhammad Adnan[2], Wakeel Ahmed[3], Muhammad Imran Faizi[4]
[1]Department of Computer Science, University of Engineering and Technology, Taxila, waqas_rizwan@hotmail.com
[2]Department of Computer Science, University of Engineering and Technology, Taxila, syed.adnan@uettaxila.edu.pk
[3] Department of Computer Science, University of Engineering and Technology, Taxila, wakeel.ahmad@uettaxila.edu.pk
[4] Department of Computer Science, University of Engineering and Technology, Taxila, imran.faizi@uettaxila.edu.pk

ABSTRACT

The skin lesion is considered the most widespread malignant disease in individuals, and melanoma is the deadliest form of the disease. Early detection affects the prognosis of the disease and improves the chances of survival. Dermatologists use scientific calculation tools such as ABCD to diagnose melanoma through visual inspection of the mole. However, computer vision tools have been presented to support the quantitative scrutiny of skin lesions. Significant improvements to deep learning algorithms in image recognition tasks should be very successful in medical image examination, particularly in the classification of skin lesions used to diagnose melanoma. In this research, a deep learning simulation with 38 layers to detect and classify skin lesions was proposed. Two datasets were used for training and testing i.e., the HAM10000 dataset & the ISIC2019 dataset. Experimental results show that the model outperforms on both the datasets hence making it nondependent of the dataset. 94.45% of validation top 3 accuracies are achieved on the HAM10000 dataset & 93.06% of validation top 3 accuracies are achieved on the ISIC2019 dataset.

Key words : Skin Lesion, Segmentation, Classification, Convolution, Pooling, Batch Normalization, Mean Absolute Error, Crossentropy, HAM10000 Dataset, ISIC2019 Dataset.

1 INTRODUCTION

Historically, the number of newly diagnosed skin cancer cases has increased by 53%. In 2018, approximately 9,320 people died of melanoma in the United States. There are 5,990 men and 3,330 women [1]. Early recognition and proper therapy of melanoma can substantially enhance patient survival.

Dermoscopy aims to improve the analysis performance of skin cancer. Dermoscopy is a non-invasive diagnostic skin imaging method that improves the visibility of skin defects. Removing reflections from the skin's surface can improve the visual effects of deep skin and stipulate insight into skin damage [2]. Dermoscopic evaluation is often used to diagnose melanoma and is more accurate than evaluation with the naked eye. However, manual examination of dermoscopy images by a dermatologist is often time-ingesting and error-prone. Even a skilled dermatologist can give a variety of diagnostic results. In this regard, the requirements for automatic identification methods are high.

Instinctive discovery of melanoma after dermoscopy imageries is a daunting task. First, it distinguishes melanoma from nonmelanoma skin lesions by differences in the shape, color, size, texture, and location of melanoma on dermoscopy images and the visual similarities between melanoma lesions and nonmelanoma lesions. It will be difficult. Second, the comparatively low contrast and blurred borders between skin lesions (particularly in the initial stages) and usual areas of the skin make the job of automatic identification difficult. Finally, the existence of natural (hair, veins) or clinical artifacts (blisters, ruler marks, color calibration tables, etc.) can hide or occlude skin lesions.

The purpose of this research is to propose effective detection and classification methods of skin lesions, which use detailed learning to identify and classify skin lesions. A 38-layer model is created for this. It compresses the input image so that the model can work efficiently and sends it to multiple layers to process the input image. The image feature processing process trains the model created on features and selects the best features for model assessment.

The rest of the paper is organized as follows: Section 2 introduces related work; Section 3 presents the proposed framework of Skin Lesion detection and classification; Section 4 describes experimental results and discusses its performance; Afterwards, the conclusion is outlined in Section 5.

Proposed a CNN model for a multiclass problem.

We recognized different types of skin diseases such as “melanoma (MEL), melanocytic nevus (NV), basal cell carcinoma (BCC), actinic keratosis / Bowens disease (intraepithelial carcinoma) (AKIEC), benign keratosis (solar lentigo / seborrheic keratosis/lichen planus-like keratosis) (BKL), dermatofibroma (DF) and vascular lesion (VASC).”

Classify the skin lesions through our CNN model.

We concluded that our CNN model gives the best results for multiclass problems.

Evaluated the proposed method on HAM10000 and ISIC 2019 datasets for skin lesion classification.

2 RELATED WORK

Thanks to the discovery and development of new methods for the precise identification of skin cancer, extensive research has been carried out in various areas.

Many tactics are employed to the skin laceration segmentation tricky, including active contour approaches [3], the threshold method [4], and other machine learning generated methods [5-9]. A common non-learning method for skin segmentation is the Otsu method [10, 11]. A strikingness-based laceration segmentation context for segmenting skin laceration areas from dermoscopic imageries was featured in [12]. The featured FGWN (Fixed Grid Wavelet Network) uses the RGB values of a dermoscopy image as input and estimates the network weights using an orthogonal least squares algorithm to optimize the system structure. The exit from the system shows the limits of the area of the skin lesions. Compared to the 7-point list, the functions obtained by the ABCD rule are computationally cheaper. The ABCD rule also confirms that the clinical diagnosis is very consistent. We see an increasing interest in the computer inspection of digital images with dermoscopy. A computer analysis strategy for images obtained with ELM (capillary emission microscopy) was established to improve the classification strategy for the early detection of melanoma [13]. A segmentation algorithm is used to extract the area of interest, and a combined function strategy associated with the functions of shape and radiation is used. Achieved sensitivity and specificity of 87% and 92%, respectively, using the KNN classifier. Recently, deep-learning methods [14], Convolutional Neural Networks (CNNs) in particular have demonstrated admirable functioning and strong simplification capabilities in numerous medical pictures assessment jobs, comprising of but not restricted to segmentation [15, 16], classification [17, 18], and detection [19, 20]. In [21] Catarina B & Jorge S. It is advisable to emulate a medical strategy and train a deep learning architecture to make a hierarchical diagnosis. Batch Normalized Convolutional Neural Networks (BN-CNN) are used to further improve the accuracy of the classification is proposed [22]. A fully automated classification procedure for skin lesions has been proposed in [23] that uses optimized depth features from many complete CNNs and different levels of abstraction. Deep learning can learn various concentrations of depiction from vivid images, and the obtained structures are extra sophisticated and are added vigorously. Another study proposed a new framework that allows the segmentation of skin lesions and automatic identification of skin cancers [24]. A unique new color wheel design (CCD) has been proposed to establish the relationship between the wavelength (λ) and the hue pattern (saturation and hue value) of the HSV. Dermoscopic images of 23 actual skin lesions (test samples), magnified with MATLAB, were segmented so that the Region of Interest (ROI) contained all suspicious regions [25]. This study describes the detection and segmentation of melanoma using a combined process of escalation and FCM. The process starts by converting the RGB image into a CIELab area. The 3D histogram of the CIELab image provides the starting value of the FCM. These are the main groups of hashing methods [26]. Various types of research recommend manual processing of images through machine learning, but the technology is very complicated. The purpose of this research is to study the effect of using CLAHE for contrast enhancement and MSRCR using CNN for contrast enhancement as a simple image processing method [27]. Another study used the PHITS Monte Carlo code to implement an algorithm that illuminates the aircraft with a standard prescription dose of 6 Gy[28]. Setiawan et al [29] K-means pool is used to study the effect of melanoma image reduction and color volume reduction on melanoma image pre-screening. The contribution of this research is to be able to select the best combination based on the accuracy of CNN's pre-screening for skin cancer. Another article containing low-power 77GHz multicolor continuous wave radar for skin cancer detection in biomedical imaging applications [30]. An efficient and inexpensive proximity probe for detecting early-stage skin cancer. Due to the tapered part, the tip of the device can reach the concentration of the electric field [31]. We proposed an extended model for the early detection of skin cancer. To reduce the waiting time for diagnosis, we use smartphones and magnifying glass as accessories for mobile devices and digitize the dermoscopy function [32].” This research provides evidence for the concept of using obstetrical neural networks to generate hyperspectral melanoma images. The adversarial generated neural network is a neural network in which two neural networks compete with each other”[33]. In another system, features of the cancer area are extracted, and a Support Vector Machine (SVM) classifier is used to identify the cancer. This diagnostic method uses images captured with dermoscopy, preprocesses the images to improve standards, de-noise the images, and then uses thresholding techniques to segment them [34]. An improved holistic learning method for classifying skin cancer. The function used is the best combination of functions extracted from different functions. H. Shape, color, texture, skeleton Lesions and then use different algorithms to classify these features Predict the class [35]. Another article proposes image processing techniques to classify skin lesions into melanoma or moles. [36]. Extracting features from skin cancer images is an important and arduous task. Automated computer diagnosis mechanism can improve accurate analysis of skin diseases, helping dermatologists shorten diagnosis time and improve patient care [37].“In [38],” Deng et al. CNN has established two branches to delete global and local structures to reach the burst limit. In [8], at first. In order to extend the implementation in image segmentation, we provide a unique loss function based on the Jaccard distance of the CNN model. Codella et al. [39] The pre-trained CNN is used as a high-level functional architecture delimiter to provide an SVM classifier after sparse coding. Osama et. al [40]presented a deep learning method that uses CAD systems and microscopic images to

fight breast cancer. The proposed method is based on the DenseNet-161 deep learning method to create a classification model. In [2], Yu et al. He built a complete foldable residual network (FCRN) to segment skin lesions, redefine image points for lesions and a new deep residual network for classification. In [41] Haroon R. & et al. investigated the possibility of obtaining binocular images of realistic skin through Adversarial Generative Network (GAN).

3 METHODOLOGY

Our proposed method consists of the following phases.

3.1. Pre-processing

The objective of the data pre-processing stage can be achieved through image enhancement, background correction, and segment the lesion images of all 7 types i.e. Actinic keratoses and intraepithelial carcinoma / Bowen's disease (akiec), basal cell carcinoma (bcc), benign keratosis-like lesions (solar lentigines / seborrheic keratoses and lichen-planus like keratoses, bkl), dermatofibroma (df), melanoma (mel), melanocytic nevi (nv) and vascular lesions (angiomas, angiokeratomas, pyogenic granulomas and hemorrhage, vasc).

3.2. Feature Extraction

This part processes the automated extraction of dermoscopic features, including both localization and classification from the segmented lesion images. CNN model consists of 38 layers.

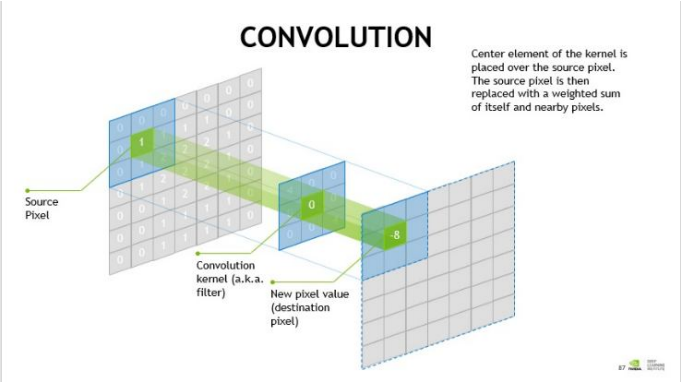

Figure 1: Convolution

3.2.1. Convolution Layer

The convolutional layer is the main component of the neural bypass network and is essentially the first layer. Figure 1 shows the folding steps. This is used to determine whether the input image has certain attributes. This is done using a bypass filter. The principle is to "drag" the window that represents the entity in the image and calculate the convolution between the entity and each part of the digitized image. Then treat that position as a candidate. In this respect the two terms are equivalent.

Therefore, the convolution layer takes multiple images as input and uses each filter to compute the convolution of each image. The filter is exactly what you are looking for in the picture.

3.3. Train Model

After the feature extraction, the model is trained to classify skin damage. At this point, the specified prototype is trained based on the training data and the results are passed on to the next step.

3.3.1. Pooling Layer

This layer is located between the two folded layers. Combine multiple feature maps, then apply the merge to each feature map. The blending process is used to reduce the image size while retaining important features. To do this, crop the image into regular cells and keep the maximum value of each cell. This study uses a 3x3 window unit and receives many input working graphics, but these working graphics are much smaller. The aggregation level reduces the number of parameters and calculations in the network. Can improve network efficiency and prevent over-modulation.

3.3.2. ReLU Layer

ReLU (Rectified Linear Unit) shows the actual non-linear function defined by ReLU (x) = max (0, x). Like that:

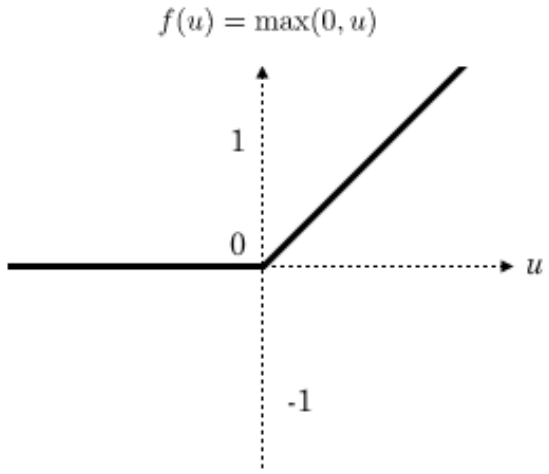

Figure 2: ReLu

The ReLU correction layer replaces all negative values received with zero. Act as an activation function.

3.3.1. Batch Normalization Layer

To improve the stability of the neural network, batch normalization subtracts the average value from the batch and then divides it by the standard deviation of the batch to normalize the output of the previous active switch.

Therefore, when normalizing the train, two trainable parameters are added to each level, the normal result is multiplied by the standard deviation factor (gamma), and then the average parameter (beta) is added. This means that SGD only changes these two weights by activation, rather than changing the attribute weights to reduce network stability at the batch level, which can provide unprecedented performance.

3.4. Score Model

The scoring model stage can control the features selected for scoring the model and send them to the next stage.

3.5. Evaluate Model

At this point, the performance and accuracy values of the model are evaluated. Help you find the best model that represents the data and how the model you choose will perform in the future.

3.6. Classification

At this point, the image is divided into different types of skin lesions.

3.6.1. Fully Connected Layer

This layer takes an input vector and creates a new output vector. Add them linearly and then apply the trigger function on the received input value.

The image as a network element was classified by the last fully connected layer. N size vector feedback. N is the number of paper ratings used to classify skin lesions. Each vector element represents the probability that the input image belongs to the category.

To calculate the probability, before using the trigger function, a fully connected level weights each input element (if N = 2;> 2, SoftMax is useful, which makes sense). This multiplies the input vector of the matrix that contains the weights. The fact that every input value is assigned to all output values explains the term "fully bound".

Figure 3 illustrates the complete picture of the methodology.

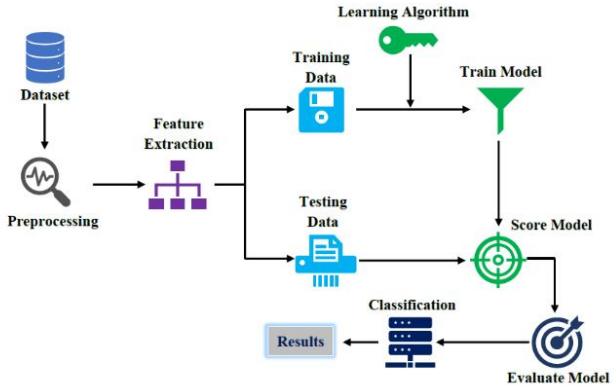

Figure 3: Methodology of Skin Lesion Classification.

4 EXPERIMENTS AND RESULTS

4.1. Dataset

In our study, we used two sets of data. The first is HAM10000, which consists of dermatoscopic images of different groups of people captured and stored in different ways. The final data set contains 10,015 dermoscopy images that will be used as a training set for academic machine learning purposes. Cases include representatives of all major diagnostic categories related to pigmented lesions: “Actinic keratoses and intraepithelial carcinoma / Bowen's disease (akiec), basal cell carcinoma (bcc), benign keratosis-like lesions (solar lentigines / seborrheic keratoses and lichen-planus like keratoses, bkl), dermatofibroma (df), melanoma (mel), melanocytic nevi (nv) and vascular lesions (angiomas, angiokeratomas, pyogenic granulomas and hemorrhage, vasc).”

The HAM10000 image dataset is organized as follows:

- **Training set**
  - 301.” Actinic keratoses and intraepithelial carcinoma / Bowen's disease (akiec) images”
  - 484 basal cell carcinoma (bcc) images
  - 1024 “benign keratosis-like lesions (solar lentigines / seborrheic keratoses and lichen-planus like keratoses, bkl) images”
  - 109 dermatofibroma (df) images
  - 1074 melanoma (mel) images
  - 5954 melanocytic nevi (nv) images
  - 131 vascular lesions (angiomas, angiokeratomas, pyogenic granulomas and hemorrhage, vasc) images

- **Test set**
  - 26 Actinic keratoses and intraepithelial carcinoma / Bowen's disease (akiec) images
  - 30 basal cell carcinoma (bcc) images
  - 75 benign keratosis-like lesions (solar lentigines / seborrheic keratoses and lichen-planus like keratoses, bkl) images
  - 06 dermatofibroma (df) images
  - 39 melanoma (mel) images
  - 751 melanocytic nevi (nv) images
  - 11 vascular lesions (angiomas, angiokeratomas, pyogenic granulomas and hemorrhage, vasc) images.

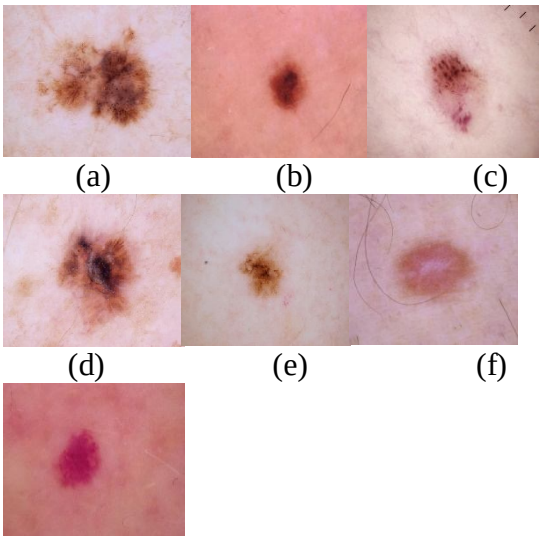

Figure 4: Examples of some skin lesions from ISIC 2018 classification challenge. (a) Melanoma (mel), (b) Melanocytic Nevus (nv), (c) Basal Cell Carcinoma (bcc), (d) Actinic Keratosis (akiec), (e) Pigmented Benign Keratosis (bkl), (f) Dermatofibroma (df) and (g) Vascular (vasc) lesions.

The second is the International Standard Industrial Classification (2019), which also includes dermoscopy images

of different groups of people, which are recorded and stored in different ways. The dataset contains 33,573 dermoscopy images that can be used as a training set for machine learning purposes. These cases include people who represent all the major diagnostic categories in the pigmented lesion area: actinic keratosis and intraepithelial carcinoma / Bowen's disease (akiec), basal cell carcinoma (CCB), benign keratosis-like lesions (actinic keratosis / seborrheic keratosis, skin fibrous keratosis (df), melanoma (mel), planar melanocytic plaque angiopathy (nv) (hematoma, angiokeratosis, pyogenic granuloma and hemorrhage, blood vessels) and squamous cell carcinoma (scc).

The ISIC image dataset is organized as follows:

- **Training set**
  - 24,177 training images.
  - ISIC_2019_Traaining_Metadata.
  - ISIC_2019_Training_GroundTruth.
- **Test set**
  - 1154 test images.
  - ISIC_2019_Test_Metadata.

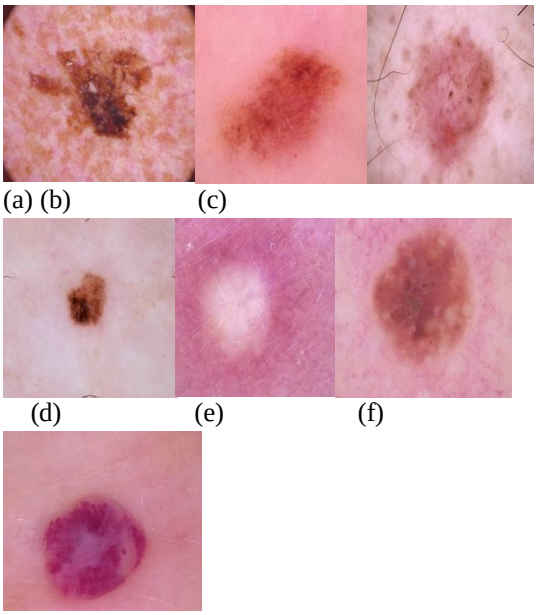

(a) (b) (c) (d) (e) (f) (g)

Figure 5: Examples of some skin lesions from ISIC 2018 classification challenge." (a) Melanoma (mel), (b) Melanocytic Nevus (nv), (c) Basal Cell Carcinoma (bcc), (d) Actinic Keratosis (akiec), (e) Pigmented Benign Keratosis (bkl), (f) Dermatofibroma (df) and (g) Vascular (vasc) lesions."

4.2. Experimental setup

Table 1: Experimental Setup

Hardware resources consist of RAM	**8GB**
Software and tools	Windows 10 Pro Education, Python
Processor Intel	core (TM) m3-7Y30 CPU @ 1.6 GHz
System type	64-bit Operating System, x64-based processor
Dataset	ISIC 2019 and HAM10000

4.3. Categorical cross-entropy

Categorical cross-entropy was used to check the distribution of prediction.

$$L\,(\,y,\hat{y}\,) = -\sum_{j=0}^{M}\sum_{i=0}^{N}\left(y_{ij} * log\,(\,\hat{y}_{ij}\,)\right)$$

Equation 1

where ŷ is the predicted value.

The entropy of the classification boundary compares the predicted distribution (activation in the output layer, one for each class) with the actual distribution. The actual class probabilities are set to 1 and the other class probabilities to 0. That is, the actual class is represented as a heat code vector.

Here are the results of categorical cross-entropy.

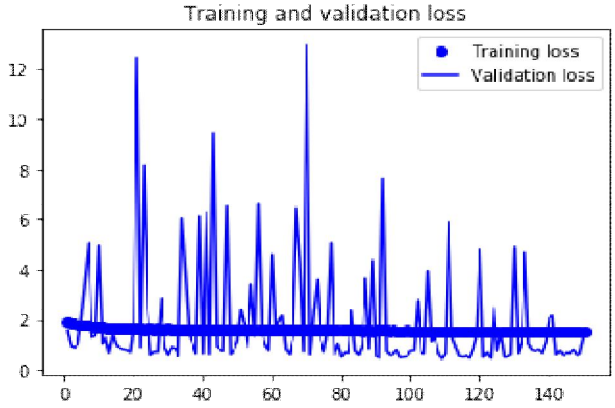

Figure 6: HAM10000 Dataset Categorical Crossentropy

HAM10000 dataset has categorical cross-entropy value = 1.3. Very little loss was shown by the model.

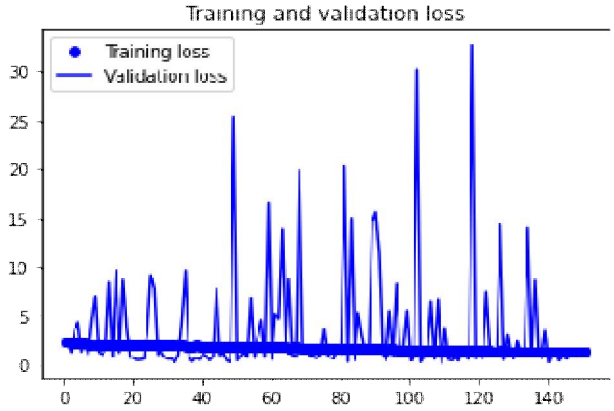

Figure 7: ISIC 2019 Dataset Categorical Crossentropy

ISIC 2019 has categorical cross-entropy value = 1.22. Little loss is shown in this dataset as well.

4.4. Mean Absolute Error

Mean Absolute Error (MAE) measures the size of the average error in a series of predictions, regardless of direction. This is the average of the absolute differences between the forecasted and real values observed in the test sample, and all individual differential weights are the same.

$$MAE = \frac{1}{n} + \sum_{j=1}^{n} |y_j - \hat{y}_j|$$

Equation 2

If no absolute values are used (error rates do not disappear), the error is the mean deviation error (MBE), which is usually used to measure the mean deviation of the model. The MBE can send useful information, but it must be interpreted because the positive and negative errors are cleared.

Here are the results of Mean Absolute Error.

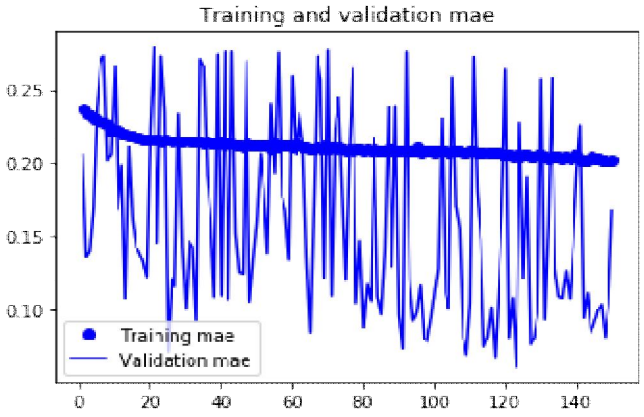

Figure 8: HAM10000 Dataset Mean Absolute Error

HAM10000 dataset has value of Mean Absolute error = 0.16. It would be less if we use a greater number of layers for our model. This is although outperforms against the state-of-the-art existing techniques.

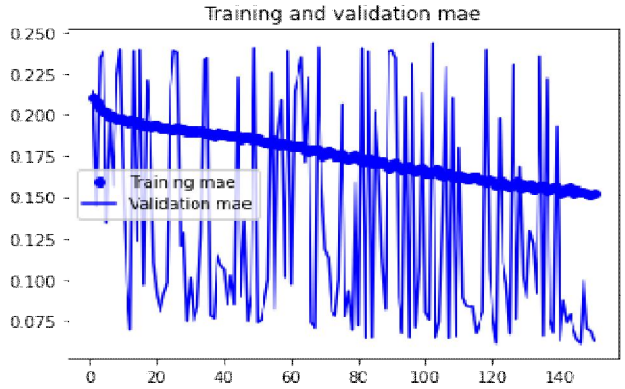

Figure 9: ISIC 2019 Dataset Mean Absolute Error

ISIC2019 dataset has a value of Mean Absolute error = 0.06. It would be less if we use a greater number of layers for our model. This is although outperforms against the state-of-the-art existing techniques.

4.5. Confusion Matrix

The confusion matrix shows the correlation between classes of skin lesions.

The confusion matrix element nij (i is a row identifier, j is a column identifier) represents the condition associated with i and is classified as j. Therefore, the elements inside the diameter (nii) were correctly classified, while the elements outside the diameter (nii) were not classified correctly. The overall figure of cases is:

$$N = + \sum_{i=1}^{M} \quad \sum_{j=1}^{M} (n_{ij})$$

Equation 3

Instead of the number of cases, the confusion matrix can be a percentage. An asymmetric confusion matrix can reveal biased classifiers.

It is clear from the confusion matrix that the NV category is overwhelmed by a large number of true positives due to a large number of images in the data set. I'm trying to use data expansion to balance the number of frames, but there are more examples in the NV category

Table 2: Confusion Matrix of HAM10000 Dataset, Without Normalization.

Akiec	3	4	2	0	1	1	3	0
Bcc	4	27	1	0	10	13	6	1
Bkl	4	8	34	0	33	38	1	0
Df	0	1	1	0	1	3	0	1
Mel	1	2	7	0	31	33	2	0
Nv	2	7	18	1	32	785	0	1
Scc	1	1	2	0	6	6	3	0
Vasc	0	1	0	0	0	4	0	7
	Akiec	**Bcc**	**Bkl**	**Df**	**Mel**	**Nv**	**Scc**	**Vasc**

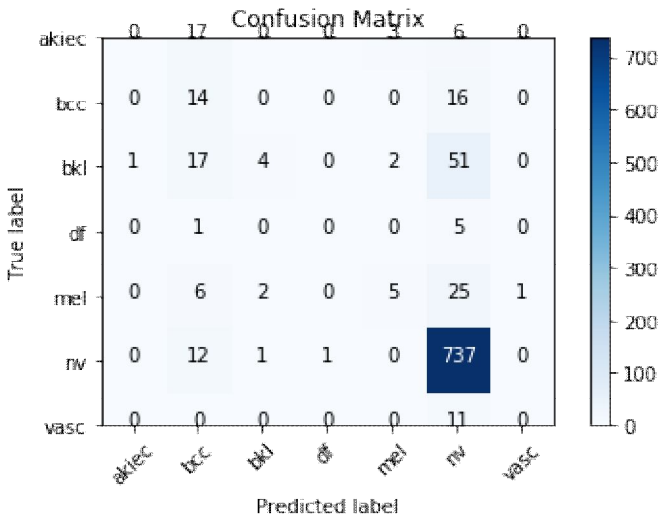

Figure 10: HAM10000 Dataset Confusion Matrix

Table 3: Confusion Matrix of ISIC2019 Dataset, Without Normalization.

Akiec	0	17	0	0	3	6	0
Bcc	0	14	0	0	0	16	0
Bkl	1	17	4	0	2	51	0
Df	0	1	0	0	0	5	0
Mel	0	6	2	0	5	25	1
Nv	0	12	1	1	0	737	0
Vasc	0	0	0	0	0	11	0
	Akiec	**Bcc**	**Bkl**	**Df**	**Mel**	**Nv**	**Vasc**

This model classifies skin lesions into different categories. The biggest challenge is an imbalanced dataset and a small amount of data. Use data expansion to reduce class imbalances and use it to provide classification accuracy scores that are not significantly distorted by a single majority class.

Table 4: Results HAM10000 Dataset

Validation Categorical Crossen tropy	0.7453487363578414
Validation Mean Absolute Error	0.12231061995418659
ValidationTop3 Accuracy	0.9445628997867804

Table 5: Results ISIC 2019 Dataset

Validation Categorical Crossen tropy	1.2264432907104492
Validation Mean Absolute Error	0.06287843734025955
ValidationTop3 Accuracy	0.9306759238243103

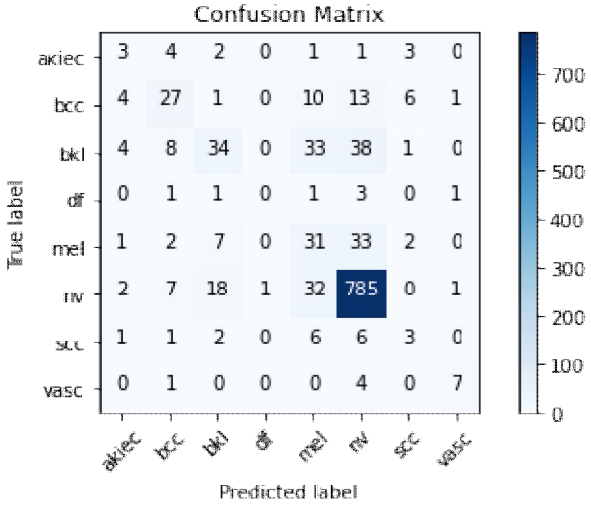

Figure 11: ISIC 2019 Dataset Confusion Matrix

5. CONCLUSION

The present article represents a supplementary argument in favor of cloud computing roles in business. This paper concludes that the Increasing role of cloud computing has many positive impacts on business in many areas like efficiency, time to market, company growth, IT and maintenance cost, etc. And decrease in Challenges for the cloud in business with the comparison of two years 2016-2017. That proves that challenges are declining very quickly. One most important thing from a business point of view is challenges are decreasing with cloud maturity. As the company matured in cloud usage, they face less difficulty as compared to cloud beginners.

AUTHORS CONTRIBUTION

All authors had approved the final version. The Corresponding Author is Waqas Rizwan.

REFERENCES

1. ***Cancer Facts & Figures 2018.*** [cited 2019 24th Oct]; Available from: https://www.cancer.org/content/dam/cancer-org/research/cancer-facts-and-statistics/annual-cancer-facts-and-figures/2018/cancer-facts-and-figures-2018.pdf.

2. Yu, L., et al., **Automated melanoma recognition in dermoscopy images via very deep residual networks**. IEEE transactions on medical imaging, 2016. **36**(4): p. 994-1004.
3. Thanh, D.N., et al., **Automatic Initial Boundary Generation Methods Based on Edge Detectors for the Level Set Function of the Chan-Vese Segmentation Model and Applications in Biomedical Image Processing,** in *Frontiers in Intelligent Computing: Theory and Applications*. 2020, Springer. p. 171-181.
4. Khambampati, A., et al., **An automatic detection of the ROI using Otsu thresholding in nonlinear difference EIT imaging**. IEEE Sensors Journal, 2018. **18**(12): p. 5133-5142.
5. Bi, L., et al., **Automatic skin lesion analysis using large-scale dermoscopy images and deep residual networks**. arXiv preprint arXiv:1703.04197, 2017.
6. Mishra, R. and O. Daescu. **Deep learning for skin lesion segmentation.** in *2017 IEEE International Conference on Bioinformatics and Biomedicine (BIBM)*. 2017. IEEE.
7. Yuan, Y., **Automatic skin lesion segmentation with fully convolutional-deconvolutional networks**. arXiv preprint arXiv:1703.05165, 2017.
8. Yuan, Y., M. Chao, and Y.-C. Lo, **Automatic skin lesion segmentation using deep fully convolutional networks with jaccard distance**. IEEE transactions on medical imaging, 2017. **36**(9): p. 1876-1886.
9. Berseth, M., *Isic 2017-skin lesion analysis towards melanoma detection.* arXiv preprint arXiv:1703.00523, 2017.
10. Thanh, D.N.H., et al. *A Skin Lesion Segmentation Method for Dermoscopic Images Based on Adaptive Thresholding with Normalization of Color Models*. in *2019 6th International Conference on Electrical and Electronics Engineering (ICEEE)*. 2019. IEEE.
11. Liu, L., et al. *Skin Lesion Segmentation Based on Improved U-net*. in *2019 IEEE Canadian Conference of Electrical and Computer Engineering (CCECE)*. 2019. IEEE.
12. Ahn, E., et al., *Saliency-based lesion segmentation via background detection in dermoscopic images.* IEEE journal of biomedical and health informatics, 2017. **21**(6): p. 1685-1693.
13. Ganster, H., et al., *Automated melanoma recognition.* IEEE transactions on medical imaging, 2001. **20**(3): p. 233-239.
14. Greenspan, H., B. Van Ginneken, and R.M. Summers, *Guest editorial deep learning in medical imaging: Overview and future promise of an exciting new technique.* IEEE Transactions on Medical Imaging, 2016. **35**(5): p. 1153-1159.
15. Havaei, M., et al., *Brain tumor segmentation with deep neural networks.* Medical image analysis, 2017. **35**: p. 18-31.
16. Ronneberger, O., P. Fischer, and T. Brox. *U-net:* **Convolutional networks for biomedical image segmentation. in International Conference on Medical image computing and computer-assisted intervention.** 2015. Springer.
17. Anthimopoulos, M., et al., **Lung pattern classification for interstitial lung diseases using a deep convolutional neural network.** IEEE transactions on medical imaging, 2016. **35**(5): p. 1207-1216.
18. Ince, T., et al., **Real-time motor fault detection by 1-D convolutional neural networks**. IEEE Transactions on Industrial Electronics, 2016. **63**(11): p. 7067-7075.
19. Dou, Q., et al., **Multilevel contextual 3-D CNNs for false positive reduction in pulmonary nodule detection**. IEEE Transactions on Biomedical Engineering, 2016. **64**(7): p. 1558-1567.
20. Dou, Q., et al., **Automatic detection of cerebral microbleeds from MR images via 3D convolutional neural networks.** IEEE transactions on medical imaging, 2016. **35**(5): p. 1182-1195.
21. Barata, C. and J.S. Marques. **DEEP LEARNING FOR SKIN CANCER DIAGNOSIS WITH HIERARCHICAL ARCHITECTURES**. in *IEEE International Symposium on Biomedical Imaging*. 2019.
22. Jayalakshmi, G. and V.S. Kumar. **Performance analysis of Convolutional Neural Network (CNN) based Cancerous Skin Lesion Detection System.** in *2019 International Conference on Computational Intelligence in Data Science (ICCIDS)*. 2019. IEEE.
23. Mahbod, A., et al. **Skin lesion classification using hybrid deep neural networks.** in *ICASSP 2019-2019 IEEE International Conference on Acoustics, Speech and Signal Processing (ICASSP)*. 2019. IEEE.
24. Adegun, A.A. and S. Viriri, **FCN-based DenseNet framework for automated detection and classification of skin lesions in dermoscopy images**. IEEE Access, 2020. **8**: p. 150377-150396.
25. Prasad, R.S., et al. **Unique color circle design for a novel Screening tool to identify cancerous skin lesions.** in *2020 IEEE International Conference on Electronics, Computing and Communication Technologies (CONECCT)*. 2020. IEEE.
26. Ganesan, P., et al. **Hill Climbing Optimization and Fuzzy C-Means Clustering for Melanoma Skin Cancer Identification and Segmentation.** in *2020 6th International Conference on Advanced Computing and Communication Systems (ICACCS)*. 2020. IEEE.
27. Setiawan, A.W. **Effect of Color Enhancement on Early Detection of Skin Cancer using Convolutional Neural Network.** in *2020 IEEE International Conference on Informatics, IoT, and Enabling Technologies (ICIoT)*. 2020. IEEE.
28. Badry, H., et al. **Dose optimization of high dose rate brachytherapy for skin cancer treatment using Harrison-Anderson-Mick applicator.** in *2020 IEEE 6th International Conference on Optimization and Applications (ICOA)*. 2020. IEEE.
29. Setiawan, A.W., A. Faisal, and N. Resfita. **Effect of Image Downsizing and Color Reduction on Skin**

Cancer Pre-screening. in *2020 International Seminar on Intelligent Technology and Its Applications (ISITIA)*. 2020. IEEE.

30. Arab, H., et al., **Early-Stage Detection of Melanoma Skin Cancer Using Contactless Millimeter-Wave Sensors.** IEEE Sensors Journal, 2020. **20**(13): p. 7310-7317.
31. Mansutti, G., et al., **Millimeter-Wave Substrate Integrated Waveguide Probe for Skin Cancer Detection**. IEEE Transactions on Biomedical Engineering, 2019. **67**(9): p. 2462-2472.
32. Poma, J.M.C., et al. **Extended Model for the Early Skin Cancer Detection Using Image Processing.** in *2020 15th Iberian Conference on Information Systems and Technologies (CISTI)*. 2020. IEEE.
33. Annala, L., et al. **Generating Hyperspectral Skin Cancer Imagery using Generative Adversarial Neural Network.** in *2020 42nd Annual International Conference of the IEEE Engineering in Medicine & Biology Society (EMBC)*. 2020. IEEE.
34. Jayade, S., D. Ingole, and M.D. Ingole. **Skin Cancer Detection Using Gray Level Co-occurrence Matrix Feature Processing.** in *2020 5th International Conference on Devices, Circuits and Systems (ICDCS)*. 2020. IEEE.
35. Sabri, M.A., et al. **Skin Cancer Diagnosis Using an Improved Ensemble Machine Learning model.** in *2020 International Conference on Intelligent Systems and Computer Vision (ISCV)*. 2020. IEEE.
36. Shayini, R. **Classification of Skin Lesions in Digital Images for the Diagnosis of Skin Cancer**. in *2020 International Conference on Smart Electronics and Communication (ICOSEC)*. 2020. IEEE.
37. Sreedhar, B., M.S. BE, and M.S. Kumar. **A Comparative Study of Melanoma Skin Cancer Detection in Traditional and Current Image Processing Techniques.** in *2020 Fourth International Conference on I-SMAC (IoT in Social, Mobile, Analytics and Cloud)(I-SMAC)*. 2020. IEEE.
38. Deng, Z., et al. **Segmentation of dermoscopy images based on fully convolutional neural network**. in *2017 IEEE International Conference on Image Processing (ICIP)*. 2017. IEEE.
39. Codella, N., et al. **Deep learning, sparse coding, and SVM for melanoma recognition in dermoscopy images**. in *International workshop on machine learning in medical imaging*. 2015. Springer.
40. Osama Mohamed, H.N., Hamdi Mahmoud, **Classification of Breast Cancer Types Based on Deep Learning Approach**. International Journal of Advanced Trends in Computer Science and Engineering, 2021. **Volume 10, No.1**.
41. Rashid, H., M.A. Tanveer, and H.A. Khan. **Skin Lesion Classification Using GAN based Data Augmentation**. in *2019 41st Annual International Conference of the IEEE Engineering in Medicine and Biology Society (EMBC)*. 2019. IEEE.